

# The Malarial Drug Target *Plasmodium falciparum* 1-Deoxy-D-Xylulose-5-Phosphate Reductoisomerase (PfDXR): Development of a 3-D Model for Identification of Novel, Structural and Functional Features and for Inhibitor Screening

Jessica L. Goble<sup>1</sup>, Matthew R. Adendorff<sup>2</sup>, Tjaart A.P. de Beer<sup>3</sup>, Linda L. Stephens<sup>1</sup> and Gregory L. Blatch<sup>1,\*</sup>

<sup>1</sup>Biomedical Biotechnology Research Unit, Department of Biochemistry, Microbiology and Biotechnology, Rhodes University, Grahamstown 6140, South Africa; <sup>2</sup>Marine Natural Products Laboratory, Department of Chemistry, Rhodes University 6140, Grahamstown, South Africa; <sup>3</sup>Bioinformatics and Computational Biology Unit, Department Biochemistry, University of Pretoria, Pretoria 0001, South Africa

**Abstract:** A three-dimensional model of the malarial drug target protein PfDXR was generated, and validated using structure-checking programs and protein docking studies. Structural and functional features unique to PfDXR were identified using the model and comparative sequence analyses with apicomplexan and non-apicomplexan DXR proteins. Furthermore, we have used the model to develop an efficient approach to screen for potential tool compounds for use in the rational design of novel DXR inhibitors.

**Keywords:** PfDXR, antimalarial, apicomplexan, inhibitors, fosmidomycin, binding affinity, IC<sub>50</sub>.

## INTRODUCTION

Human malaria can be caused by four different species of *Plasmodium* protozoa, namely *Plasmodium malariae*, *Plasmodium ovale*, *Plasmodium vivax* and *Plasmodium falciparum*, with the latter being the most deadly species [1]. In 2006, 109 countries were classified as areas at risk of malaria, with 189 to 327 million clinical cases and 610 000 to 1 212 000 deaths being reported in that year [2].

Because of the increasing problem of antimalarial drug resistance, the need for new and effective drugs against existing targets, and new targets, is also escalating [3]. Numerous approaches are being taken to identify novel antimalarial targets, such as strategies that target unique aspects of the parasite biology, for example, apicoplast targets [4]. Apicomplexans are obligatory intracellular parasites that spend a part of their life cycle within the host. They are characterized by the presence of a specialised organelle, the apicoplast, located at the apices of cells, and which contains enzymes that are involved in penetrating host tissues [5].

Exploitation of apicoplast biology for drug discovery involves manipulation of the biochemical pathways that are present in bacteria, plants and apicomplexan parasites, but not in the human host [6]. Numerous biochemical pathways in *P. falciparum* have been identified as new potential drug targets, one of which is the mevalonate/non-mevalonate pathway for isoprenoid biosynthesis [3].

Isoprenoids are the most chemically diverse group of compounds present in all organisms and have essential roles in membrane structure, redox chemistry, reproductive cycles, growth regulation, signal transduction and defense mechanisms [7]. Isopentenyl pyrophosphate (IPP) is the general precursor required for isoprenoid biosynthesis, which occurs via either the mevalonate (MVA) or mevalonate-independent (MEP) pathway [9]. Organisms such as mammals and fungi use the MVA pathway for isoprenoid biosynthesis [10], while numerous bacteria, green algae, and higher plants utilize the alternative MEP pathway [9]. Because of the crucial role that isoprenoids play in survival of organisms, the synthetic steps involved in isoprenoid biosynthesis could be targeted in antimalarial drug design [11].

The MEP pathway is comprised of seven enzymatic steps, which begins with the formation of 1-deoxy-D-xylulose-5-phosphate (DXP) by condensation of pyruvate and glyceraldehyde [12]. The subsequent step is catalyzed by 1-deoxy-D-xylulose-5-phosphate reductoisomerase (DXR) and involves an intramolecular rearrangement and NADPH-dependent reduction of DXP to MEP (2-C-methyl-erythritol 4-phosphate) [13].

The *Escherichia coli* DXR enzyme has been well documented in the literature [14, 8, 15], with the crystal structures revealing information about enzyme function. They revealed that DXR assembles as a homodimer [14] and that substrate specificity is maintained by the existence of a flexible loop covering the substrate binding site; the flexible loop was also implicated in playing an important role in the enzymatic reaction [8].

Not long after the discovery of DXR, reports of natural inhibitors emerged; the most potent inhibitor was found to be

\*Address correspondence to this author at the Department of Biochemistry, Microbiology and Biotechnology, Rhodes University, Grahamstown 6140, South Africa; Tel: +27-46-603-8262; Fax: +27-46-622-3984; E-mail: g.blatch@ru.ac.za

an antibacterial agent called fosmidomycin [16]. Replacement of the formyl-hydrogen (H) of fosmidomycin by a methyl group (CH<sub>3</sub>) yielded the inhibitor FR900098 [17]. The crystal structure of *Ec*DXR, with Mn<sup>2+</sup> and fosmidomycin bound, provided evidence that fosmidomycin binds in a fashion closely related to the substrate DXP [18]. To date, several DXR inhibitors have been identified [19-23], fosmidomycin and its analogue FR900098 have been shown to be the most potent. Yet despite significant progress, these compounds have been shown to exhibit reduced pharmacological properties and their potential to become drugs is considered poor [24].

In the absence of an experimentally determined structure, it is important that an appropriate *Pf*DXR model be established to facilitate predictions about its structure-function and inhibitor binding properties. This approach has been used previously and a *Pf*DXR model was developed and successfully used for *in silico* docking studies with various inhibitors, including fosmidomycin and FR900098 [25]. However, this model was not made publically available and there were very few *Pf*DXR inhibitor binding studies available (fosmidomycin and FR900098) [19] for the authors to use in validation of their model. Since this *Pf*DXR modelling study, further experimental inhibitor binding studies have been conducted on *Pf*DXR [23]. This provides an opportunity to produce a more vigorously validated *Pf*DXR model for use in further structure, function and inhibitor screening studies.

In this work, a three-dimensional homology model for *Pf*DXR has been created using MODELLER. The model has been verified by way of a Ramachandran plot and using docking-based validation. The *Pf*DXR active site has been rigorously analysed, so that a structure-based approach can be taken for determination of novel inhibitors. This was accomplished by comparative docking of more than 30 ligands into *Pf*DXR and *Ec*DXR, as well as using statistical analyses of binding affinity versus experimental IC<sub>50</sub> inhibition values from the literature. Furthermore, using comparative sequence and structure analysis with apicomplexan and non-apicomplexan DXR proteins, structural and functional features unique to *Pf*DXR were identified.

## MATERIALS AND METHODS

### Primary Validation and Structural Analysis of the Predicted Active Site of *Pf*DXR

It can be assumed that the tertiary structure of two proteins is similar if their sequences share a significant degree of similarity [26]. Medium-accuracy comparative models are based on 30 to 50% sequence identity [27]. After sequence alignment, the *Pf*DXR homology model was created in MODELLER (version 9v2) [28], using the crystal structures of *Escherichia coli* DXR (1Q0Q.pdb) [15], *Zymomonas mobilis* DXR (1R0K.pdb) [29] and *E.coli* IspC (1ONP.pdb) [18], where 36.2, 36.6 and 35.2 % sequence similarity respectively was found. The multiple sequence alignment was completed in ClustalX [30] and the obtained alignment was manually inspected and edited before quality checks were done. The initial *Pf*DXR model was energy minimized using the *InsightIII*/DISCOVER module, with 500 steps of steepest decent, at 22°C. The homology model was assessed using

WHATIF (version 6.0), PROCHECK [31, 32] and the Ramachandran plot. Model images were rendered using PyMOL (version 0.98) [33] and Accelrys Visualizer/Material Studios (version 2.0) (www.accelrys.com). The coordinates of the *Pf*DXR homology model are freely available; please contact the corresponding author (g.blatch@ru.ac.za).

### Comparative Sequence Analysis for Prediction of Function

The 417 amino acid sequence of *Pf*DXR (accession number: XM\_001348779.1) minus the leader peptide was used in this study. The 72 amino acid leader peptide comprises a unique N-terminal extension that resembles a 30 amino acid endoplasmic reticulum signal peptide and a 44 amino acid peptide sequence characteristic of a plastidial targeting sequence [34]. Sequence alignments were derived using the ClustalW v.1.8 package [35]. The BLOSUM matrices were used to score the alignments, with the parameters for 'gap open', 'gap extension', and 'gap distance' set at 10, 0.5, and 8, respectively. The DXR homologues against which the *Pf*DXR was aligned included: *Plasmodium vivax* (accession number: XM\_001615665), *Plasmodium berghei* (accession number: XM\_673952), *Plasmodium yoelii* (accession number: XM\_720958), *Arabidopsis thaliana* (accession number: AJ242588), *Z.mobilis* (accession number: 1R0K\_A) and *E.coli* (accession number: 1JVS\_A). The obtained alignments were manually inspected to ensure consistency with known structural information. Gene Runner (version 3.1) was used to analyse sequences with respect to open reading frames, composition and motif searches.

### Docking-based Model Validation and Inhibitor Screening

Docking studies were performed on an Intel Core 2 Duo 3GHz workstation, equipped with OCZ 8800GTX 768MB DDR3 graphics. From the reference crystal structure for *Ec*DXR (1Q0L.pdb) [15], fosmidomycin was removed from the binding site and the molecule was desolvated; the NADPH cofactor was retained in the structure. The protocol was validated by docking the minimized fosmidomycin structure into the original protein crystal structure (1Q0L). The ligands were sketched in Accelrys Visualizer/Material Studios (version 2.0), with the phosphonate moieties in the deprotonated state and minimized at the B3LYP/6-31G(d) level using Gaussian 03 (www.gaussian.com). Non-polar hydrogens were merged using the Autodock 4.0 tool set, and all permitted torsions were allowed in the docking studies. The protein active site and surrounding residues were mapped using the AutoGrid 4.0 algorithm, incorporating a grid box of dimensions 60 x 60 x 60 units along the x, y and z axes, respectively. Atom maps were generated for all potential interactions between the ligand and the active site residues, where catalytic residues were kept flexible (Ser186, Ser222, Asn227, Lys228, Glu231 for *Ec*DXR; Ser199, Ser235, Asn240, Lys241, Glu244 in *Pf*DXR). The dockings were executed using a Lamarckian algorithm in AutoDock 4.0 [36] to create populations containing 150 individuals and allowing for a maximum of 2.5 x 10<sup>6</sup> energy evaluations. For each ligand, 10 docks were generated, with visual analysis and ligand scoring data being used to decide upon the optimal conformation for each docking run.

## RESULTS AND DISCUSSION

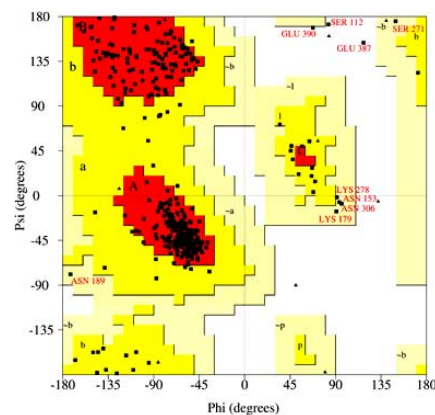
### Primary Validation of the Predicted PfDXR Model

According to the NCBI database, there are 21 three-dimensional molecular structures for the DXR enzyme available [37], none of which are from the *P. falciparum* homologue. Only one research group has to date, published a validated PfDXR homology model [25]; however, the coordinates of this model are not publically available.

Following sequence alignment, a predicted PfDXR three-dimensional structure was generated using MODELLER, with optimization and minimization using InsightII/DISCOVER. The first measure for model verification involved tertiary structure assessment using WHATIF and WHAT CHECK. The Ramachandran plot of psi and phi backbone conformational angles for each residue in the protein can be seen in Fig. (1A) and a normal distribution is apparent. The data from the Ramachandran plot is summarised in Fig. (1B), and it is evident that the PfDXR model is comparable to the EcDXR crystal structure (1Q0L.pdb), with respect to most favoured regions (87.4 %), generously allowed regions (10.3 %), and additionally allowed regions (1.5 %); as well as for the stereochemical quality of the model, as observed using the PROCHECK protein structure checking programme. Only three residues (0.8 %) were in disallowed conformations and these include Ser112, Glu387 and Glu390 (Fig. 1A and 1B). With respect to the protein secondary structure, all three disallowed conformations were only fractionally out of the generously allowed region. All three residues are located on a surface loop, suggesting that they would be unlikely to modify the internal protein core or secondary structure of the protein. The superimposition of the predicted PfDXR homology model and EcDXR (1Q0L.pdb) showed that PfDXR shares a similar homology with the known EcDXR crystal structure (Fig. 1C). In conclusion, the proposed PfDXR model was sufficiently validated to be subjected to structure–function analysis of its active site and to ligand docking studies. The latter were also used to further validate the model.

### Comparative Sequence Analysis for Prediction of Function

Protein targeting in malaria parasites involves numerous compartments and is highly complex [38]. Examples of known targeting methods in *P. falciparum* include post-translational addition of a GPI anchor [39], sorting by timing [40], oligosaccharide-mediated signalling (glycosylation) [41], and targeting via motifs embedded in the amino acid sequence of the protein [38]. The best-studied example of amino acid motif-based targeting is the apicoplast, which functions in fatty acid biosynthesis [42, 19]. Even though trafficking to the apicoplast is better understood than with other compartments, much remains unknown [46]. Most proteins of the apicoplast are encoded in the nucleus and are imported into the apicoplast following post-translational modification [38]. Numerous *P. falciparum* proteins contain an N-terminal hydrophobic region (signal peptide) that functions to target the secretory pathway [43]. Studies have confirmed that further signalling is required for transport to the apicoplast, over and above targets into the secretory system; this is known as a sub-terminal targeting system [44, 45].



|  | EcDXR      | PfDXR       |
|--|------------|-------------|
| Total Number of Residues                 | 398        | 417         |
| Most favoured regions [A,B,L]            | 332 (93 %) | 339 (87.4%) |
| Generously allowed regions [-a,-b,-l,-p] | 24 (6.7 %) | 40 (10.3%)  |
| Additional allowed regions [a,b,l,p]     | 1 (0.3 %)  | 6 (1.5%)    |
| Disallowed regions [XX]                  | 0 (0 %)    | 3 (0.8%)    |
| Glycine residues                         | 21         | 15          |
| Proline residues                         | 18         | 13          |
| End-residues (excl. Gly & Pro)           | 2          | 1           |
| Overall Score (PROCHECK)                 | 0.19       | -0.48       |
| Mainchain G-factor Score                 | 0.20       | -0.72       |

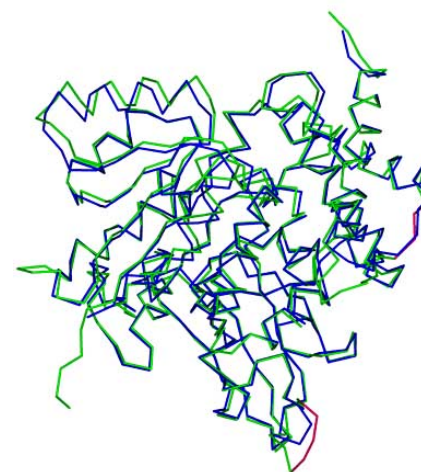


**Figure 1.** (A) Conformational map (Ramachandran plot) of the psi and phi backbone conformational angles for each residue in the modelled PfDXR, where “most favoured” (coloured in red), “generously allowed” (yellow), “additionally allowed” (beige), and “disallowed” (white) regions are described. (B) Ramachandran plot statistics for EcDXR crystal structure (1Q0L.pdb) and PfDXR homology model. The overall PROCHECK score of >0.50 is recommended and investigation is needed for a score <-1.0. The G-factor score is a measure of the overall normality of the structure and is the average of all the different G-factors for each residue in the structure. (C) Schematic view of the PfDXR homology model (coloured in green) superimposed onto the crystal structure of EcDXR (1Q0L.pdb) (blue), with only alpha carbons shown in a wire frame. Motifs on the protein surface that occur at sequence insert regions on PfDXR are coloured pink. Hydrogens are not shown.

A colour version of this figure is available online at [www.bentham.org/ppl/MSand1.htm](http://www.bentham.org/ppl/MSand1.htm)

Targeting motifs are readily interchangeable [44, 45] however, no obvious amino acid motifs have been identified; it has been speculated that evidence for these motifs might lie

in the secondary or three-dimensional tertiary structures [46], where mutagenesis experiments may provide some information regarding the residues that are important for trafficking [38].

Analysis of the amino acid sequence alignment in Fig. (2), revealed that PfDXR, as well as the other apicomplex-

ans, contained sequence insertions that were not evident in the bacterial and plant homologues. These insertions appeared at the following positions on the PfDXR sequence: residues 30–32, 184–193 and 382–384 (Figs. 2 and 3B). At residues 291–293 on the AtDXR sequence (305–307 on the PfDXR sequence), the plant homologue contained an insertion that did not appear in any of the other homologues (Fig.

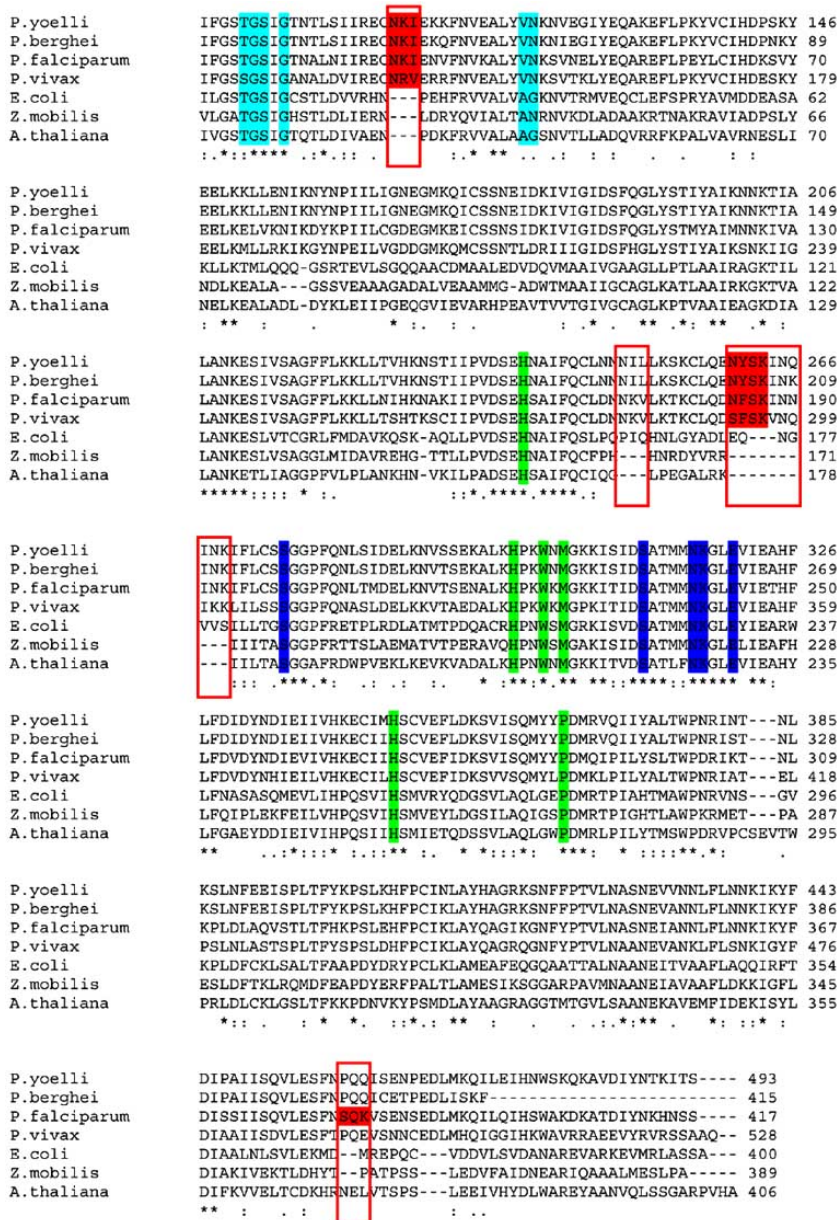


**Figure 2.** Multiple sequence alignment of *P.falciparum* DXR using ClustalW AND BLOSUM matrices for scoring. The consensus sequence characterizes identical residues as ‘\*’, strongly similar residues as ‘:’ and weakly similar residues as ‘.’. Residues are highlighted according to catalytic or structural function and include: residues that bind NADPH cofactor (highlighted in light blue), structural residues important in active site formation (green) and catalytic residues (blue). Sequence insert regions specific to apicomplexans appear in blocks (coloured red), with N-glycosylation sites (NFSK/NYSK) and protein kinase C phosphorylation site (SQK) within insert region coloured red. Alignment was performed with homologous sequences from other organisms, namely: *Plasmodium vivax* (accession number: GI: 156099974), *Plasmodium berghei* (accession number: GI:68074258), *Plasmodium yoelii* (accession number: GI:82595927), *Arabidopsis thaliana* (accession number: GI:4886306), *Zymomonas mobilis* (accession number: GI:51247274) and *Escherichia coli* (accession number: GI:24987413). All sequences are truncated forms that do not include portions of the N-terminus. A colour version of this figure is available online at [www.bentham.org/pp/MSandI.htm](http://www.bentham.org/pp/MSandI.htm)

**3B).** When the *PfDXR* sequence was inspected for potential motifs, a potential N-glycosylation site (N-{P}-[ST]-{P}) at residues 382–384 and protein kinase C (PKC) phosphorylation site ([ST]-x-[RK]) at residues 184–187, were coded for within sequence insertion regions (Fig. 3A). The other apicomplexans share the same N-glycosylation motif at the same alignment position; however the PKC phosphorylation motif is specific to the *PfDXR* homologue (Fig. 2).

Although glycosylation appears to be rare in *P. falciparum*, a basic N-glycosylation pathway does exist [47]. The potential N-glycosylation site presents itself on an extended loop region of *PfDXR* (Figs. 1C and 3A). The occurrence of this motif at the protein surface suggests that it could potentially be an active glycosylation site. Glycosylation at this motif may facilitate protein folding or improved solubility [48]. Alternatively, it may be involved in *PfDXR* targeting to the apicoplast after it has moved through the secretory pathway [48]. N-linked glycosylation occurs in both eukaryotes and archaea, but very rarely in bacteria [49]. This may be a rationale for the absence of the motif in the *EcDXR* sequence at a surface position, as per Fig. (2). Other *Plasmodium* apicomplexans, which include *P.yoelli*, *P.berghei* and *P.vivax*, exhibit an N-glycosylation motif at the same position as *P.falciparum* (Fig. 2). Interestingly, the position of

the motif consistent with all apicomplexa appears at an insertion region that is not a feature of the bacterial or plant homologues. Experimental evidence suggests that *P. falciparum* possess both a secretory and glycosylation pathway [50, 47] that involves trafficking of apicoplast–destined proteins through four membranes, resulting from the secondary endosymbiotic origin of the apicoplast [38]. This may be a potential reason for the evolution of the sequence insertions in the *Plasmodium* species.

The cellular location of a target protein, as well as enzyme activity and associations with other proteins can be altered through phosphorylation by protein kinases [51]. Protein kinases play a functional role in a multitude of processes, including cell proliferation, division, differentiation and apoptosis [52]. *PfDXR* potentially boasts a surface PKC phosphorylation motif at a region of sequence insertion (Figs. 2 and 3A). The motif, however, was not predicted to occur on an extended loop, as was predicted for the N-glycosylation motif (Fig. 1C). None of the other homologues showed evidence of the motif at a similar position, suggesting that this may be an attribute specific to *PfDXR* (Fig. 2). Experimentally, PKC demonstrates a preference for the phosphorylation of serine/threonine when these residues are located close to a C-terminal basic residue [53, 54]. The

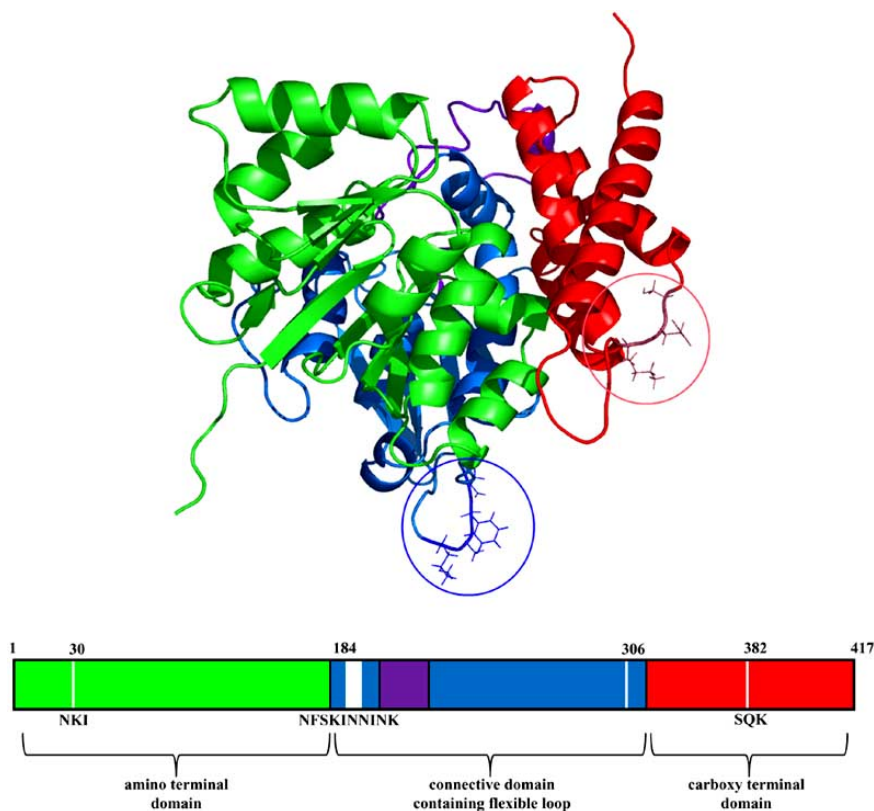


**Figure 3.** (A) Ribbon representation of *PfDXR* monomer coloured by domain: amino terminal dinucleotide binding domain (coloured green), a connective domain (blue) which includes a 30 residue flexible loop (purple), and a carboxy terminal four-helix bundle domain (red). Motifs on the protein surface that occur at sequence insert regions are highlighted, where an N-glycosylation site (NFSK) (dark blue) and a protein kinase C phosphorylation site (SQK) (raspberry) are shown in sticks. (B) Linear representation of *PfDXR* monomer (417 residues) coloured by domain, with the location of the insert regions labelled by residue position (relative to *PfDXR*) and residue name. The *PfDXR* insert regions occur at residue positions 30, 184 and 382 and residues are labelled appropriately. At residue 306, *AtDXR* presents an insert that does not appear in other homologues. A colour version of this figure is available online at [www.bentham.org/pp1/MSandL.htm](http://www.bentham.org/pp1/MSandL.htm)

PKC phosphorylation motif of *PfDXR* contains only a single C-terminal basic lysine, suggesting that it may be a relatively poor substrate for PKC (Fig. 2). In conclusion, information can be obtained from sequence and structural analyses of *PfDXR* that may provide a link between its structure and function.

### Structural Analysis of the Predicted Active Site of *PfDXR*

The *EcDXR* enzyme presents itself as an 86 kDa homodimer, with three domains making up each monomer [8]; these include an amino-terminal dinucleotide binding domain (residues 1–150), a carboxyl terminal four-helix bundle (residues 328–400) [14], and a connective domain, which accommodates most of the active site and is also involved in dimerisation of the enzyme [8]. The *PfDXR* model proposed here presents itself as a 46.7 kDa v-shaped monomer, as is seen with the *EcDXR* homologue (Figs. 1C and 3A) [8]. The connective domain also contains a flexible loop or “hatch” that is said to move over the active site after the substrate has bound [14]. According to Fig. (2), the residues that correspond to these regions in the *P.falciparum* sequence are as follows: residues 1–160 in the *PfDXR* sequence comprises the amino terminal domain; residues 161–340, the connective domain; and residues 341–417 make up the carboxyl terminal domain; the position of the three domains can be viewed in Figs. (3A and 3B). As with the proposed *EcDXR* models in the literature [14, 8, 15], the connective domain of

the *PfDXR* model also accommodates all of the active site residues, namely Ser199, Ser235, Asn240, Lys241, Glu244 (Ser186, Ser222, Asn227, Lys228, Glu231 in *EcDXR*) (Fig. 4A and 4B) [14, 18]. According to the available literature, the catalytic loop or hatch, as well as the nicotinamide moiety of NADPH are both required for the correct positioning of the active site [18]. In particular, Trp212 and Met214 in *EcDXR* (Trp225 and Met227 in *PfDXR*) perform a vital stacking role when the active site is shaped (Figs. 4A and 4B) [18]. Upon docking of various inhibitors into *EcDXR*, it became evident that Met276 closed over the active site as a potential substitute for Met214 (Figs. 4A and 4B); this trend was not seen in *PfDXR* docking studies. This potential *EcDXR* structural substitution is also documented in the literature [18]. Other structurally significant residues in *EcDXR* include His153, His209, His257 and Pro274 (His163, His222, His270 and Pro287 in *PfDXR*), which are essential in the formation of the active site architecture [18, 14]. It is evident in Figs. (4A and 4B) that the architecture of the *EcDXR* and *PfDXR* active sites are very similar, where the catalytic residues and structural residues named have very similar orientations and positions.

The active sites of both homologues are indeed similar; however differences in the hatch residues are evident, where Asp211 and Ser213 are both replaced with lysine residues in *PfDXR* (Fig. 4A and 4B). The substitutions of the small polar asparagine and serine residues in *EcDXR* for large basic lysines in *PfDXR* are fairly non-conservative substitutions.

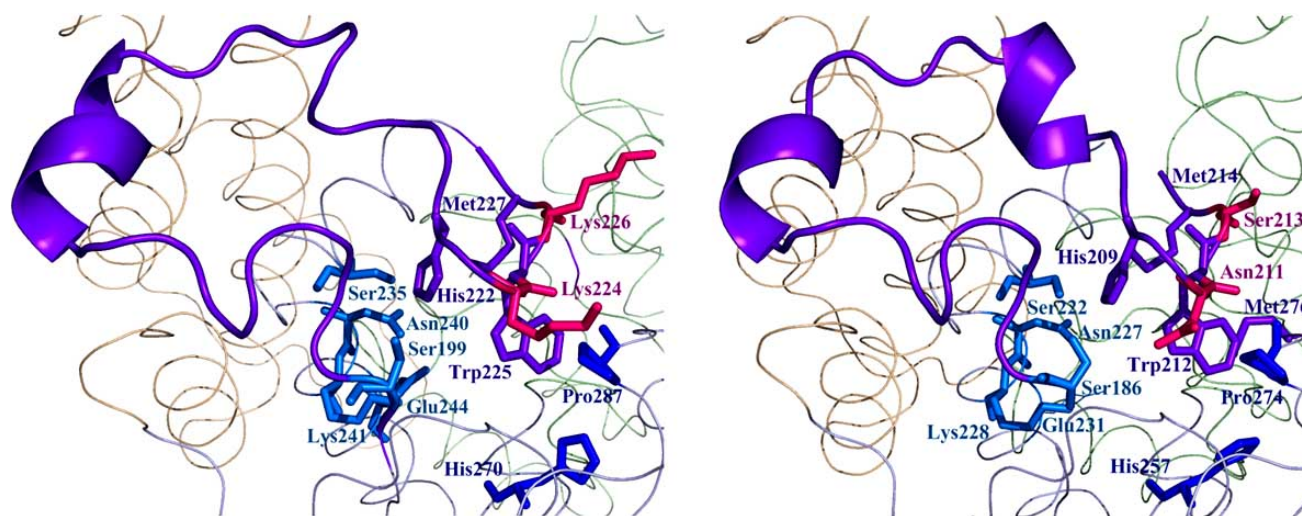


**Figure 4.** (A) Stick representation of *PfDXR* monomer coloured by domain, zoomed into the catalytic site: amino terminal dinucleotide binding domain (coloured pale green), connective domain (pale blue) which includes a 30 residue flexible loop (shown in ribbon representation and coloured purple), and carboxy terminal four-helix bundle domain (pale red). The side chains for hatch residues His222, Trp225 and Met227 are shown (coloured purple). The Lys224 and Lys226 residues are shown in sticks because they are different in size and charge when compared to the *E. coli* homologue (pink). Catalytic residues that are shown in stick include: Ser199, Ser235, Asn240, Lys241 and Glu244 (light blue). Structural residues that are shown in stick include: His270, Pro287 (blue). Hydrogens are not shown. (B) Stick representation of *EcDXR* monomer coloured by domain, zoomed into the catalytic site: amino terminal dinucleotide binding domain (coloured pale green), connective domain (pale blue) which includes a 30 residue flexible loop (shown in ribbon representation and coloured purple), and carboxy terminal four-helix bundle domain (pale red). The side chains for hatch residues His209, Trp212 and Met214 are shown (coloured purple). In some docking studies, Met276 (purple) has been shown to close over the active site instead of Met214. The Lys224 and Lys226 residues (in *PfDXR*) are substituted with Asn211 and Ser213 in the *E. coli* homologue (pink). Catalytic residues that are shown in stick include: Ser186, Ser222, Asn227, Lys228 and Glu231 (light blue). Structural residues that are shown in stick include: His257, Pro274 (blue). Hydrogens are not shown. A colour version of this figure is available online at [www.bentham.org/pp/MSandI.htm](http://www.bentham.org/pp/MSandI.htm)

Asn211 is within 9.56 Å of the ligand and similarly, Lys224 is within 9.15 Å of the docked ligand FR900098, for *EcDXR* and *PfDXR* respectively (Fig. S1; see supporting information), meaning that no direct intermolecular interactions are possible. The difference in the bulkiness of the side chains may result in the *PfDXR* catalytic hatch behaving in a slightly modified manner to that of other species'. Ser213 in *EcDXR* and Lys226 in *PfDXR* do not appear to form part of the active site architecture as they exist at the C-terminal portion of the hatch. It is however evident that upon binding of the inhibitor and cofactor to *PfDXR*, movement of Lys226 occurs; this may be to facilitate movement of NADPH into the active site (Figs. S2B and S2C; see supporting information). According to Fig. (S2A) (see supporting information), hydrogen bonding interactions between Ser213 and Ser12, as well as between Asn211 and Ser254/Pro252 exist when FR900098 and NADPH are docked into *EcDXR*. Upon entry of FR900098 and NADPH into *PfDXR*, a hydrogen bonding interaction between Pro223 and the side chain nitrogen of Lys224 takes place (Fig. S2B; see supporting information). However, when no ligands are docked into the *PfDXR*, the position of Lys224 is significantly different and no noted hydrogen bonding interactions occur (Fig. S2C; see supporting information). It can hence be concluded that upon binding of an inhibitor and cofactor, the *PfDXR* hatch changes conformation significantly in order to facilitate its movement over the active site, as is noted in the literature [14].

In *EcDXR*, NADPH cofactor binding includes: backbone amides of Gly11 and Ser12 (Gly16 and Ser17 in *PfDXR*), which coordinate the pyrophosphonate moiety [8]; Ala35 and Gly36 (Val43 and Asn44 in *PfDXR*) which accommodate the 2' phosphate [8]; Thr10 (Thr15 in *PfDXR*), which anchors the 2' phosphonate moiety [14]; and Gly14 (Gly19 in *PfDXR*), which forms an important part of the NADPH binding motif [8, 55]. All these catalytically and structurally significant residues, that are involved in binding the substrate/ inhibitor or cofactor, are highly conserved among bacterial (*E. coli*, *Z. mobilis*), plant (*A. thaliana*) and other apicomplexan homologues (*P. vivax*, *P. berghei*, *P. yoelii*) (Fig. 2). In *EcDXR*, NADPH demonstrates 9 hydrogen bonding interactions, which include the residues Thr10, Ser12, Ile13, Lys37, Asn38, Ile101, Lys125 and Gly215. With *PfDXR*, similar protein-cofactor interaction are observed, with hydrogen bonding of the protein to residues Gly16, Ser17, Ile18, Asn44, Ser46, Asp111 and Asn133 (Gly11, Ser12, Ile13, Gly36, Val102 and Asn124 in *EcDXR*). Superimposition of the docked cofactor into *EcDXR* and into *PfDXR* confirmed that the orientation of NADPH in both homologues was comparable (data not shown). It was hence concluded that the protein-cofactor interactions are similar for the *EcDXR* and *PfDXR* homologues.

### Docking-Based Model Validation and Inhibitor Screening

The reliability of the docking protocol was validated by removing fosmidomycin from *EcDXR* (1QOL.pdb), and then redocking it into the protein, as well as into the modelled *PfDXR* the modelled *PfDXR*. Similarly, this protocol was applied to 30 other ligands; for each docking run, 10 possible docks were generated. The best docking mode was chosen

based on the greatest number of interactions, orientation of the ligand in the active site, and the binding affinity. Structurally similar ligands, *i.e.* from the same research group, exhibited similar orientations.

All ligands were quantified with respect to binding affinity and the number of hydrogen bonding interactions. The theoretical inhibition potential of each ligand was graphically classified into quadrants; this can be seen in Fig. (5). According to Fig. (5A and 5B), those ligands that demonstrated lowest binding energy (Kcal/mol) versus highest incidence of interaction included: LTB95, LD\_2\_6, FR900098, LD\_1\_1, KD562, UK213, TK85, LD\_2\_7, UK721, fosmidomycin and LTB65 for *EcDXR*; and LTB95, 2a, TK85, UK721, fosmidomycin, FR900098 and LD\_2\_7 for *PfDXR*. In all the above mentioned docking simulations, interactions between their phosphonate moiety and N-formyl oxygen, with the respective proteins were documented (see Fig. S3, supporting information for structures).

It is evident from Fig. (5) that those ligands which have been reported to be efficient at inhibiting DXR, such as FR900098 and fosmidomycin, reside within the expected quadrant. This further validates the *PfDXR* homology model proposed and provides a novel methodology for virtual screening. This method of quantification therefore provides an efficient methodology available to screen for potential tool compounds, for use in the rational design of novel DXR inhibitors.

In the case of the phosphate mimics 24a-h [23],  $\alpha$ -substituted fosmidomycin analogues [22] and DXR inhibitors [21], it was evident that a phosphonate moiety carrying a significant negative charge, as well as a nitrogen atom carrying a partial/induced negative charge, was required for reasonable binding of the active site residue; this has also been documented in the literature for fosmidomycin and FR900098 in a DFT study, which quantified the partial charges for each atom of the respective inhibitors [56]. This nitrogen atom can come in the form of an N-formyl nitrogen. The presence of these charged or partially charged groups, as compared to the carbon atom, may provide an active site environment suitable for tight binding. When the 3'-amido-3'-deoxy-N<sup>6</sup>-(1-naphthylmethyl) adenosine derivatives 9a-d [20] were docked into *EcDXR* and *PfDXR*, very few hydrogen bonding interactions were observed (data not shown). The ligands from this group are not bulky and therefore entered the active site efficiently, yielding a reasonable binding affinity. The apparent lack of hydrogen bonding means that the ligands may move freely between the active site and external environment. The lack of hydrogen bonding may be directly related to the lack of a highly charged nitrogen atom and phosphonate moiety in the structures. Given this, it is surprising that the compounds of this group still displayed moderate antimalarial activity against *P. falciparum* (micromolar range) and some inhibitory activity against DXR [20]. The activity was however weak when compared to fosmidomycin, which has been shown to have antimalarial activity against *P. falciparum* in the nanomolar range [19, 22, 23].

Binding affinity was then plotted against experimental IC<sub>50</sub>, as shown in the Figs. (5A and 5B) inserts; this provides a model against which one can differentiate between active

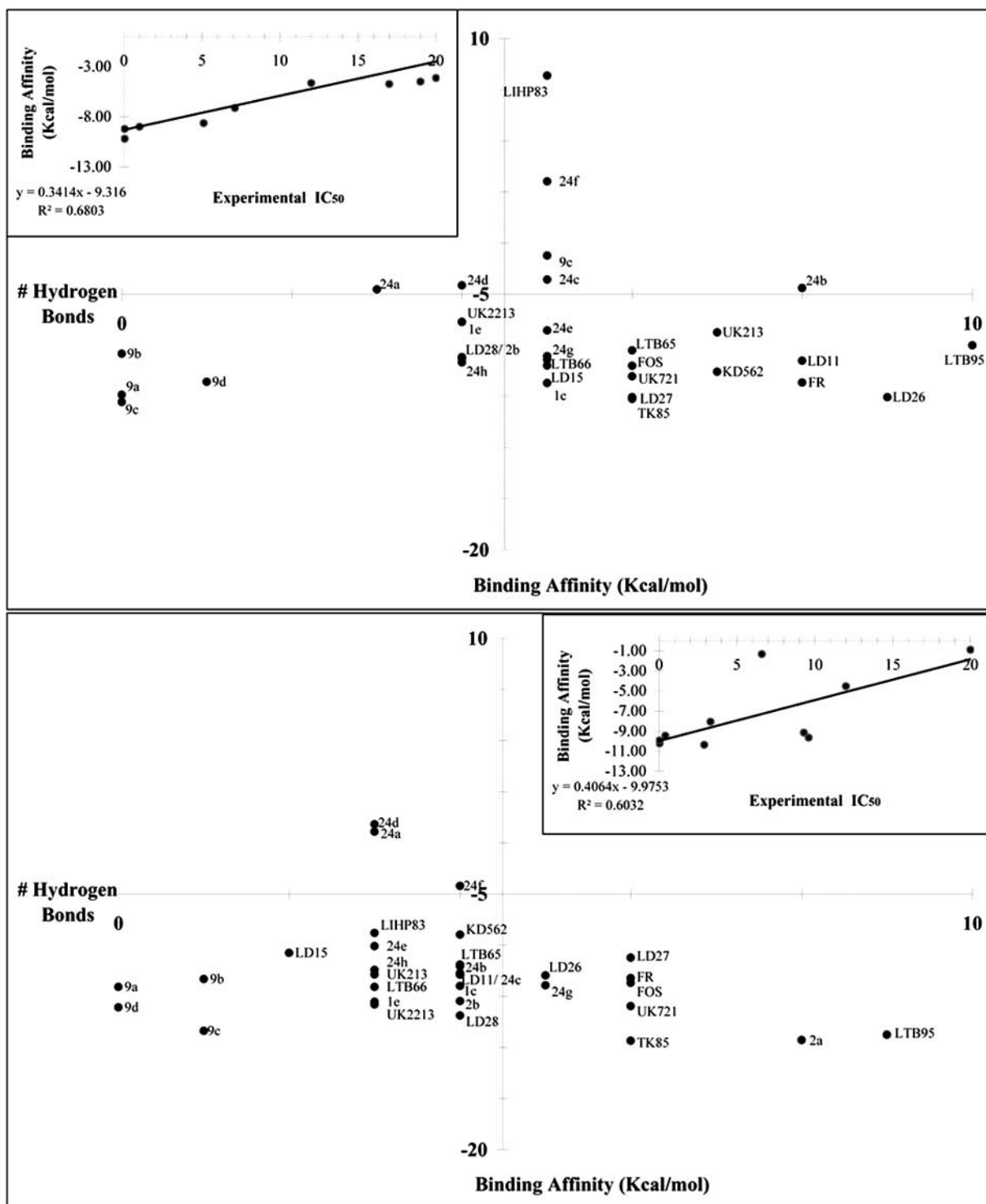


**Figure 5.** (A) For *EcDXR*, graph showing the correlation between binding affinity (in Kcal/mol) and the number of hydrogen bonds for 32 potential DXR inhibitors docked into *EcDXR*. Inhibitors include: Fosmidomycin, FR900098, DXR inhibitors KD562, LD<sub>1\_1</sub>, LD<sub>1\_5</sub>, LD<sub>2\_6</sub>, LD<sub>2\_7</sub>, LD<sub>2\_8</sub>, LIHP<sub>83</sub>, LTB65, LTB66, LTB95, TK85, UK213, UK2213, UK721 [21], 3'-amido-3'-deoxy-N<sup>6</sup>-(1-naphthylmethyl) adenosine 9a–d [20],  $\alpha$ -substituted fosmidomycin analogues 1c, 1e, 2a, 2b [22], non-hydrolyzable phosphate mimics 24a–h [23]. The potential DXR inhibitors are classified into one of four quadrants: top left, poor binding affinity with poor hydrogen bonding; top right, poor binding affinity with good hydrogen bonding; bottom left, good binding affinity with poor hydrogen bonding; bottom right, good binding affinity with good hydrogen bonding. (insert A) Graph showing a correlation between binding affinity (in Kcal/mol) and known experimental IC<sub>50</sub> value determined by Gießmann *et al.* (2008) for Fosmidomycin, FR900098 and non-hydrolyzable phosphonate mimics

(Legend Fig. 5) contd...

24a–h docked into *Ec*DXR. **(B)** For *Pf*DXR, graph showing the correlation between binding affinity (in Kcal/mol) and the number of hydrogen bonds for 32 potential DXR inhibitors docked into *Pf*DXR. Inhibitors include: Fosmidomycin, FR900098, DXR inhibitors KD562, LD\_1\_1, LD\_1\_5, LD\_2\_6, LD\_2\_7, LD\_2\_8, LIHP\_83, LTB65, LTB66, LTB95, TK85, UK213, UK2213, UK721 [21], 3'-amido-3'-deoxy-N<sup>6</sup>-(1-naphthylmethyl) adenosine 9a–d [20],  $\alpha$ -substituted fosmidomycin analogues 1c, 1e, 2a, 2b [22], non-hydrolyzable phosphate mimics 24a–h [23]. The potential DXR inhibitors are classified into one of four quadrants: top left, poor binding affinity with poor hydrogen bonding; top right, poor binding affinity with good hydrogen bonding; bottom left, good binding affinity with poor hydrogen bonding; bottom right, good binding affinity with good hydrogen bonding. (insert B) Graph showing a correlation between binding affinity (in Kcal/mol) and known experimental IC<sub>50</sub> value determined by Gießmann *et al.* (2008) for fosmidomycin, FR900098 and non-hydrolysable phosphonate mimics 24a–h docked into *Pf*DXR.

and inactive inhibitors. According to the Figs. **(5A)** and **(5B)** inserts, *Ec*DXR demonstrated a reasonable correlation of 0.68, while *Pf*DXR showed a less significant correlation between binding affinity and IC<sub>50</sub> of 0.60. From these trends it can be concluded that the DXR enzyme does not accommodate ligands boasting bulky side chains. This may be because the side chains of active site residues protrude into the active site binding pocket, potentially creating a highly charged environment; this can be seen in Fig. **(4)**. Those ligands with bulky side chains can engage in intramolecular bonding to facilitate entry into the active site (data not shown); in some cases, ligands conformationally altered from the minimized state. As an example, in Fig. **(6C)**, when 24g was docked into *Pf*DXR, the ligand adopted a reasonable linear arrangement comparable with that of the minimized ligand. When docked into *Ec*DXR, 24g assumed an entirely new conformation, as can be seen in Fig. **(6D)**; where the *Ec*DXR backbone, with 24g docked, was superimposed onto the *Pf*DXR backbone equivalent such that the protein orientation was identical.

When fosmidomycin was docked into *Pf*DXR the phosphonate moiety of the ligand interacted with the following residues: Ser199, Ser235, Asn240 and Lys241 in *Pf*DXR (Ser186, Ser222, Asn227 and Lys228 in *Ec*DXR). Rather than a direct interaction, Glu244 in *Pf*DXR (Glu231 in *Ec*DXR), played a supporting role to stabilise the catalytic lysine (data not shown). In the literature, interactions with Gly197 (Gly200 in *Pf*DXR) and His219 (His222 in *Pf*DXR) have been observed for the *Pf*DXR–NADPH–fosmidomycin complex [25]. These interactions were not observed upon fosmidomycin docking, they were however observed upon docking of other ligands; *i.e.* FR900098 and 24f (for Gly200) docked into *Pf*DXR; interactions with FR900098 include: Ser199, Ser235, Asn240, Lys241 and Gly200 for *Pf*DXR, and Ser186, Ser222, Asn227, Lys228, Glu231, Ser151 and Gly185 for *Ec*DXR, as observed in Figs. **(6A)** and **(6B)** respectively. Similarly, interactions with 24g and UK2213 were also apparent (for His222) when docked into *Pf*DXR. The hydrogen bonding interaction between His209 (His222 in *Pf*DXR) and the phosphonate moiety of the substrate is said to be the reason for the closing of the hatch once the substrate has entered [55, 14], shielding the reactants completely from the solvent environment [8]. As in the literature, when FR900098 was docked into *Ec*DXR and *Pf*DXR, the ligand maintained a similar orientation to that of fosmidomycin (data not shown) [25].

In a recent study by Gießmann *et al.* (2008), IC<sub>50</sub> values ( $\mu$ M) were obtained for fosmidomycin, FR900098 and a

range of other non-hydrolyzable phosphate mimics using an NADPH-dependent assay. The study concluded that FR900098 was two to three times more active against the malaria parasite than fosmidomycin; Fosmidomycin was shown to have similar inhibition in the malaria parasite and bacteria [23]. In this study, fosmidomycin and FR900098 maintained similar binding affinities, ligand efficiencies and number of hydrogen bonds, as demonstrated in Figs. **(5A)** and **(5B)** for *Ec*DXR and *Pf*DXR respectively [23].

Coupled with fosmidomycin and FR900098, the docking of other non-hydrolysable phosphate mimics (24a–h) into *Ec*DXR and *Pf*DXR was used for docking-based validation of the *Pf*DXR model. Statistically, the difference in order of magnitude, for *Ec*DXR and *Pf*DXR experimental IC<sub>50</sub> values, should be consistent with computational binding affinities. For example, the binding affinities for 24c docked into *Ec*DXR and *Pf*DXR was –4.15 and –12.16 Kcal/mol respectively; this meant that theoretically *Pf*DXR had a 2.9-fold greater inhibition potential because it utilized significantly less energy to bind at the active site. Experimentally, 24c was found to demonstrate a 2.2-fold higher inhibition of *Pf*DXR when compared to *Ec*DXR [23]. The other phosphate mimics (24a–h), demonstrated the same trend (data not shown), indicating that the theoretical *Pf*DXR model behaves in the same manner as the *Pf*DXR enzyme does experimentally.

In conclusion, the *Pf*DXR theoretical model, through binding energy estimates, may provide some evidence of the potential inhibitory strength (IC<sub>50</sub>) of novel inhibitor compounds. The *Pf*DXR model can also be used to screen compound libraries for the identification of potential inhibitors, or for the identification of tool compounds from which novel inhibitors can be rationally designed.

## CONCLUSION

The proposed *Pf*DXR model was sufficiently validated to be subjected to structure–function analysis of its active site and to ligand docking studies. Analysis of the primary and secondary structure of *Pf*DXR, other apicomplexan and non-apicomplexan DXR's, resulted in identification of structural and functional features unique to *Pf*DXR. Ligand docking studies provided structural information regarding movement of the hatch upon inhibitor binding, and showed that there were significant differences in *Pf*DXR when compared to *Ec*DXR. The validated model was also used to develop an efficient screening method for potential tool compounds for use in the rational design of novel DXR inhibitors, where potential inhibitory strength (IC<sub>50</sub>) may be estimated.

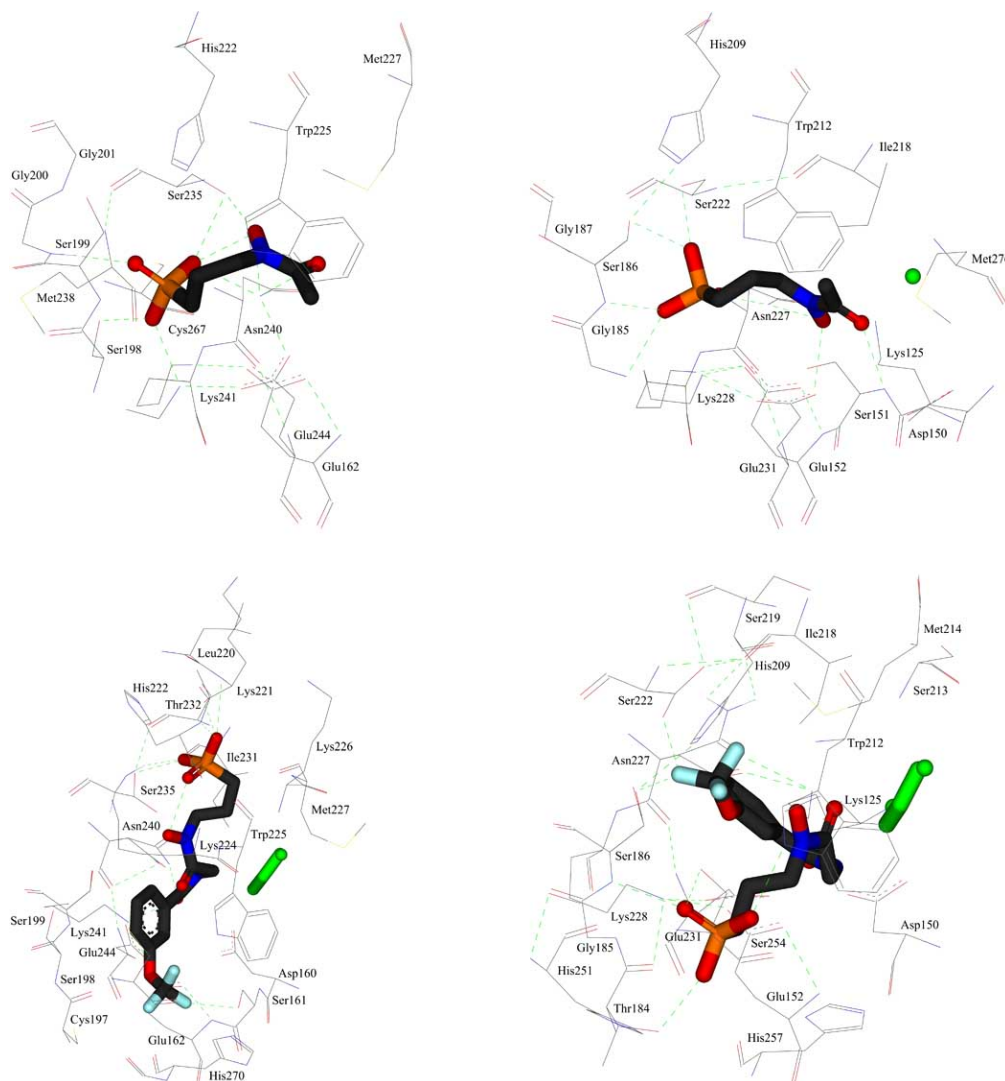


**Figure 6.** (A) Schematic view of FR900098 bound to *PfDXR* active site. Residues within 4 Å of the ligand are shown and labelled and hydrogen bonds are dotted in green. (B) Schematic view of FR900098 bound to *EcDXR* (1Q0L) active site (identical orientation to that of *PfDXR* with FR900098 bound). Residues within 4 Å of the ligand are shown and labelled and hydrogen bonds are dotted in green. Those atoms of NADPH within 4 Å of the ligand are shown in solid green. (C) Schematic view of phosphate mimic 24g bound to *PfDXR* active site. Residues within 4 Å of the ligand are shown and labelled and hydrogen bonds are dotted in green. Those atoms of NADPH within 4 Å of the ligand are shown in solid green. (D) Schematic view of phosphate mimic 24g bound to *EcDXR* (1Q0L) active site (identical orientation to that of *PfDXR* with 24g bound). Residues within 4 Å of the ligand are shown and labelled and hydrogen bonds are dotted in green. Those atoms of NADPH within 4 Å of the ligand are shown in solid green. A colour version of this figure is available online at [www.bentham.org/pp/MSandl.htm](http://www.bentham.org/pp/MSandl.htm)

#### ACKNOWLEDGEMENTS

We are grateful to Delia Tanner who contributed to this work in early stages of the study, to Professor P. Kaye, Dr K. Lobb and Dr A. Ö. Tastan Bishop for their intellectual input, and to the South African Malaria Initiative (SAMI) who supported this work. The authors declare that there is no conflict of interest in this work.

#### ABBREVIATIONS

DXP = 1-Deoxy-D-xylulose-5-phosphate  
 IspC = 1-Deoxy-D-xylulose-5-phosphate reductoisomerase

*PfDXR* = *Plasmodium falciparum* 1-deoxy-D-xylulose-5-phosphate reductoisomerase  
*EcDXR* = *Escherichia coli* 1-deoxy-D-xylulose-5-phosphate reductoisomerase  
*ZmDXR* = *Zymomonas mobilis* 1-deoxy-D-xylulose-5-phosphate reductoisomerase  
*AtDXR* = *Arabidopsis thaliana* 1-deoxy-D-xylulose-5-phosphate reductoisomerase

|                  |   |                                       |
|------------------|---|---------------------------------------|
| MVA pathway      | = | Mevalonate pathway                    |
| MEP pathway      | = | Mevalonate-independent pathway        |
| MEP              | = | 2-C-methyl-erythritol 4-phosphate     |
| PKC              | = | Protein kinase C                      |
| IC <sub>50</sub> | = | Half maximal inhibitory concentration |
| Kcal/mol         | = | Kilo calories per mole                |
| GPI              | = | Glycosylphosphatidylinisitol          |
| Ala (A)          | = | Alanine                               |
| Arg (R)          | = | Arginine                              |
| Asn (N)          | = | Asparagine                            |
| Asp (D)          | = | Aspartic acid                         |
| Cys (C)          | = | Cysteine                              |
| Glu (E)          | = | Glutamic acid                         |
| Gly (G)          | = | Glycine                               |
| His (H)          | = | Histidine                             |
| Ile (I)          | = | Isoleucine                            |
| Leu (L)          | = | Leucine                               |
| Lys (K)          | = | Lysine                                |
| Met (M)          | = | Methionine                            |
| Phe (F)          | = | Phenylalanine                         |
| Pro (P)          | = | Proline                               |
| Ser (S)          | = | Serine                                |
| Thr (T)          | = | Threonine                             |
| Trp (W)          | = | Tryptophan                            |
| Tyr (Y)          | = | Tyrosine                              |
| Val (V)          | = | Valine                                |
| Å                | = | Angstroms                             |

## SUPPORTING INFORMATION AVAILABLE

Analysis of the hatch upon binding of FR900098 into EcDXR and PfDXR, showing differences (Fig. S1 and S2); as well as the chemical structures of inhibitors used for docking studies (Fig. S3).

## SUPPLEMENTARY MATERIAL

Supplementary material is available on the publishers Web site along with the published article.

## REFERENCES

- [1] World Health Organisation, WHO. Malaria: Fact sheet number 94, 2007 (available online at <http://www.who.int/mediacentre/factsheets/fs094/en/print.html>).
- [2] World Health Organisation, WHO. World Malaria Report, Nonserial Publication, 2008. (summary available online at <http://www.who.int/malaria/wmr2008/WMR08-news-summary.pdf>).
- [3] Macreadie, I.; Ginsburg, H.; Sirawaraporn, W.; Tilley, L. Antimalarial drug development and new targets. *Parasitol. Today*, **2000**, *16*, 438-444.
- [4] Rosenthal, P.J. Review: Antimalarial drug discovery: old and new approaches. *J. Exp. Biol.*, **2003**, *206*, 3735-3744.
- [5] Morrisette, N.S.; Silbey, L.D. Cytoskeleton of apicomplexan parasites. *Microbiol. Mol. Biol. Rev.*, **2002**, *66*, 21-38.
- [6] Roos, D.S.; Crawford, M.J.; Donald, R.G.; Fraunholz, M.; Harb, O.S.; He, C.Y.; Kissinger, J.C.; Shaw, M.K.; Striepen, B. Mining the Plasmodium genome database to define organellar function: what does the apicoplast do? *Philos. Trans. R. Soc. Lond. B. Biol. Sci.*, **2002**, *357*, 35-46.
- [7] Rodriguez-Concepcion, M.; Campos, N.; Lois, L.M.; Maldonado, C.; Hoefler, J.F.; Grosdemange-Billiard, C.; Rohmer, M.; Boronat, A. Genetic evidence of branching in the isoprenoid pathway for the production of isopentenyl diphosphate and dimethylallyl diphosphate in *Escherichia coli*. *FEBS Lett.*, **2000**, *473*, 328-332.
- [8] Reuter, K.; Sanderbrand, S.; Jomaa, H.; Wiesner, J.; Steinbrecher, I.; Beck, E.; Hintz, M.; Klebe, G.; Stubbs, M. Crystal structure of 1-deoxy-D-xylulose 5-phosphate reductoisomerase, a crucial enzyme in the nonmevalonate pathway of isoprenoid biosynthesis. *J. Biol. Chem.*, **2002**, *277*, 5378-5384.
- [9] Disch, A.; Schwender, J.; Müller, C.; Lichtenthaler, H.K.; Rohmer, M. Distribution of the mevalonate and glyceraldehyde phosphate/pyruvate pathways for isoprenoid biosynthesis in unicellular algae and the cyanobacterium *Synechocystis* PCC 6714. *Biochem. J.*, **1998**, *333*, 381-388.
- [10] Vial, H.J.; Philippot, J.R.; Wallach, D.F. A re-evaluation of the status of cholesterol in erythrocytes infected by *Plasmodium knowlesi* and *P. falciparum*. *Mol. Biochem. Parasitol.*, **1984**, *13*, 53-65.
- [11] Dubey, V.S. Mevalonate-independent pathway of isoprenoids synthesis: A potential target in some human pathogens. *Curr. Sci.*, **2000**, *83*, 685-688.
- [12] Takahashi, S.; Kuzuyama, T.; Watanabe, H.; Seto, H. A 1-deoxy-D-xylulose 5-phosphate reductoisomerase catalyzing the formation of 2-C-methyl-D-erythritol 4-phosphate in an alternative nonmevalonate pathway for terpenoid biosynthesis. *Proc. Natl. Acad. Sci. USA*, **1998**, *95*, 9879-9884.
- [13] Argyrou, A.; Blanchard, J.S. Kinetic and chemical mechanism of *Mycobacterium tuberculosis* 1-deoxy-D-xylulose-5-phosphate isomerase. *Biochemistry*, **2004**, *43*, 4375-4384.
- [14] Yajima, S.; Nonaka, T.; Kuzuyama, T.; Seto, H.; Ohsawa, K. Crystal structure of 1-deoxy-D-xylulose 5-phosphate reductoisomerase complexed with cofactors: implications of a flexible loop movement upon substrate binding. *J. Biochem. (Tokyo)*, **2002**, *131*, 313-317.
- [15] Mac Sweeney, A.; Lange, R.; Fernandes, R.P.; Schulz, H.; Dale, G.E.; Douangamath, A.; Proteau, P.J.; Oefner, C. The crystal structure of *E. coli* 1-deoxy-D-xylulose-5-phosphate reductoisomerase in a ternary complex with the antimalarial compound fosmidomycin and NADPH reveals a tight-binding closed enzyme conformation. *J. Mol. Biol.*, **2005**, *345*, 115-127.
- [16] Kuzuyama, T.; Shimizu, T.; Takahashi, S.; Seto, H. Fosmidomycin, a specific inhibitor of 1-deoxy-D-xylulose 5-phosphate reductoisomerase in the nonmevalonate pathway for terpenoid biosynthesis. *Tetrahedron Lett.*, **1998**, *39*, 7913-7916.
- [17] Okuhara, M.; Kuroda, Y.; Goto, T.; Okamoto, M.; Terano, H.; Kohsaka, M.; Aoki, H.; Imanaka, H. Studies on new phosphonic acid antibiotics: III. Isolation and characterization of FR-31564, FR-32863 and FR-33289. *J. Antibiot.*, **1980**, *33*, 24-28.
- [18] Steinbacher, S.; Kaiser, J.; Eisenreich, W.; Huber, R.; Bacher, A.; Rohdich, F. Structural basis of fosmidomycin action revealed by the complex with 2-C-methyl-D-erythritol 4-phosphate synthase (IspC). Implications for the catalytic mechanism and anti-malaria drug development. *J. Biol. Chem.*, **2003**, *278*, 18401-18407.
- [19] Jomaa, H.; Wiesner, J.; Sanderbrand, S.; Altincicek, B.; Weidemeyer, C.; Hintz, M.; Turrbachova, I.; Eberl, M.; Zeidler, J.; Lichtenthaler, H.; Soldati, D.; Ewald Beck, E. Inhibitors of the nonmevalonate pathway of isoprenoid biosynthesis as antimalarial drugs. *Science*, **1999**, *285*, 1573-1576.
- [20] Herforth, C.; Wiesner, J.; Heidler, P.; Sanderbrand, S.; Van Calenbergh, S.; Jomaa, H.; Link, A. Antimalarial activity of N<sup>6</sup>-substituted adenosine derivatives. Part 3. *Bioorg. Med. Chem.*, **2004**, *12*, 755-762.
- [21] Silber, K.; Heidler, P.; Kurz, T.; Klebe, G. AFMoC enhances predictivity of 3D QSAR: A case study with DOXP-reductoisomerase. *J. Med. Chem.*, **2005**, *48*, 3547-3563.
- [22] Haemers, T.; Wiesner, J.; Van Poecke, S.; Goeman, J.; Henschker, D.; Beck, E.; Jomaa, H.; Van Calenbergh, S. Synthesis of  $\alpha$ -substituted fosmidomycin analogues as highly potent *Plasmodium*

- falciparum* growth inhibitors. *Bioorg. Med. Chem. Lett.*, **2006**, *16*, 1888-1891.
- [23] Gießmann, D.; Heidler, P.; Haemers, T.; Van Calenbergh, S.; Reichenberg, A.; Jomaa, H.; Weidemeyer, C.; Sanderbrand, S.; Wiesner, J.; Link, A. Towards new antimalarial drugs: synthesis of non-hydrolyzable phosphate mimics as feed for a predictive QSAR study on 1-deoxy-D-xylulose-5-phosphate reductoisomerase inhibitors. *Chem. Biodivers.*, **2008**, *5*, 643-656.
- [24] Singh, N.; Cheve, G.; Avery, M.A.; McCurdy, C.R. Targeting the methyl erythritol phosphate (MEP) pathway for novel antimalarial, antibacterial and herbicidal drug discovery: inhibition of 1-deoxy-D-xylulose-5-phosphate reductoisomerase (DXR) enzyme. *Curr. Pharm. Des.*, **2007**, *13*, 1161-1177.
- [25] Singh, N.; Cheve, G.; Avery, M.A.; McCurdy, C.R. Comparative protein modeling of 1-deoxy-D-xylulose-5-phosphate reductoisomerase enzyme from *Plasmodium falciparum*: a potential target for antimalarial drug discovery. *J. Chem. Inf. Model.*, **2006**, *46*, 1360-1370.
- [26] Kroemer, R.T.; Doughty, S.W.; Robinson, A.J. Prediction of the three-dimensional structure of human interleukin-7 by homology modelling. *Protein Eng.*, **1996**, *9*, 493-498.
- [27] Baker, D.; Sali, A. Protein structure prediction and structural genomics. *Science*, **2001**, *294*, 93-96.
- [28] Sali, A.; Blundell, T.L. Comparative protein modelling by satisfaction of spatial restraints. *J. Mol. Biol.*, **1993**, *234*, 779-815.
- [29] Ricagno, S.; Grolle, S.; Bringer-Meyer, S.; Sahn, H.; Lindqvist, Y.; Schneider, G. Crystal structure of 1-deoxy-D-xylulose-5-phosphate reductoisomerase from *Zymomonas mobilis* at 1.9-Å resolution. *Biochim. Biophys. Acta*, **2004**, *1698*, 37-44.
- [30] Thompson, J.D.; Gibson, T.J.; Plewniak, F.; Jeanmougin, F.; Higgins, D.G. The ClustalX windows interface: flexible strategies for multiple sequence alignment aided by quality analysis tools. *Nucl. Acids Res.*, **1997**, *24*, 4876-4882.
- [31] Vriend, G. WHAT IF: a molecular modelling and drug design program. *J. Mol. Graph.*, **1990**, *8*, 52-56.
- [32] Laskowski, R.A.; MacArthur, M.W.; Moss, D.S.; Thornton, J.M. PROCHECK: a program to check the stereochemical quality of protein structures. *J. Appl. Crystallogr.* **1993**, *26*, 283-291.
- [33] DeLano, W.L. *The PyMOL molecular graphics system*. DeLano Scientific: San Carlos, CA, U.S.A. **2002**.
- [34] Schwartzbach, S.D.; Osafune, T.; Löffelhardt, W. Protein import into cyanelles and complex chloroplasts. *Plant Mol. Biol.* **1998**, *38*, 247.
- [35] Thompson, J.D.; Higgins, D.G.; Gibson, T.J. CLUSTAL W: Improving the sensitivity of progressive multiple sequence alignment through sequence weighting, position-specific gap penalties and weight matrix choice. *Nucl. Acids Res.*, **1994**, *22*, 4673-4680.
- [36] Morris, G.M.; Goodsell, D.S.; Halliday, R.S.; Huey, R.; Hart, W.E.; Belew, R.K.; Olson, A.J. Automated docking using a Lamarckian genetic algorithm and empirical binding free energy function. *J. Comput. Chem.*, **1998**, *19*, 1639-1662.
- [37] National Center for Biotechnology Information, NCBI, **2008** (available online at [http://www.ncbi.nlm.nih.gov/sites/ query? term=1-deoxy-D-xylulose-5-phosphate+reductoisomerase](http://www.ncbi.nlm.nih.gov/sites/query?term=1-deoxy-D-xylulose-5-phosphate+reductoisomerase)).
- [38] van Dooren, G.G.; Waller, R.F.; Joiner, K.A.; Roos, D.S.; McFadden, G.I. Traffic Jams: protein transport in *Plasmodium falciparum*. *Parasitol. Today*, **2000**, *16*, 421-427.
- [39] Karsten, V.; Qi, H.; Beckers, C.J.M.; Reddy, A.; Dubremetz, J.F.; Webster, P.; Joiner, K.A. The protozoan parasite *Toxoplasma gondii* targets proteins to dense granules and the vacuolar space using both conserved and unusual mechanisms. *J. Cell Biol.*, **1998**, *141*, 1323-1333.
- [40] Le Cabec, V.; Cowland, J.B.; Calafat, J.; Borregaard, N. Targeting of proteins to granule subsets is determined by timing and not by sorting - the specific granule protein NGAL is localized to azurophilic granules when expressed in HL-60 cells. *Proc. Natl. Acad. Sci. U. S. A.*, **1996**, *93*, 6454-6457.
- [41] Dahms, N.M.; Lobel, P.; Kornfeld, S. Mannose 6-phosphate receptors and lysosomal enzyme targeting. *J. Biol. Chem.*, **1989**, *264*, 12115-12118.
- [42] Waller, R.F.; Keeling, P.J.; Donald, R.G.K.; Striepen, B.; Handman, E.; Lang-Unnasch, N.; Cowman A.F.; Besra, G.S.; Roos, D.S.; McFadden, G.I. Nuclear-encoded proteins target to the plastid in *Toxoplasma gondii* and *Plasmodium falciparum*. *Proc. Natl. Acad. Sci. USA*, **1998**, *95*, 12352-12355.
- [43] von Heijne, G. Signal sequences: the limits of variation. *J. Mol. Biol.*, **1985**, *184*, 99-105.
- [44] McFadden, G.I. Plastids and protein targeting. *J. Euk. Microbiol.*, **1999**, *46*, 339-346.
- [45] McFadden, G.I. Endosymbiosis and evolution of the plant cell. *Curr. Opin. Plant Biol.*, **1999**, *2*, 513-519.
- [46] Wien, H.L.J.; Czisch, M.; de Kruijff, B. The structural flexibility of the preferredoxin transit peptide. *FEBS Lett.*, **1999**, *453*, 318-326.
- [47] Templeton, T.J.; Iyer, L.M.; Anantharaman, V.; Enomoto, S.; Abrahamte, J.E.; Subramanian, G.M.; Hoffman, S.L.; Abrahamson, M.S.; Aravind, L. Comparative analysis of apicomplexa and genomic diversity in eukaryotes. *Genome Res.*, **2004**, *4*, 1686-1695.
- [48] Fournillier, A.; Wychowski, C.; Boucreux, D.; Baumert, T.F.; Meunier, J.C.; Jacobs, D.; Muguet, S.; Depla, E.; Inchauspe, G. Induction of hepatitis C virus E1 envelope protein-specific immune response can be enhanced by mutation of N-glycosylation sites. *J. Virol.*, **2001**, *75*, 12088-12097.
- [49] Marshall, R.D. Glycoproteins. *Annu. Rev. Biochem.*, **1972**, *41*, 673-702.
- [50] Gowda, D.C.; Davidson, E.A. Protein glycosylation in the malaria parasite. *Parasitol. Today*, **1999**, *15*, 147-152.
- [51] European Molecular Biology Laboratory, EMBL, European Bioinformatics Institute, **2008** (available online at <http://www.ebi.ac.uk/interpro/DisplayProEntry?ac=IPR001495>).
- [52] Manning, G.; Plowman, G.D.; Hunter, T.; Sudarsanam, S. Evolution of protein kinase signaling from yeast to man. *Trends Biochem. Sci.*, **2002**, *27*, 514-20.
- [53] Woodgett, J.R.; Gould, K.L.; Hunter, T. Substrate specificity of protein kinase C. Use of synthetic peptides corresponding to physiological sites as probes for substrate recognition requirements. *Eur. J. Biochem.*, **1986**, *161*, 177-184.
- [54] Kishimoto, A.; Nishiyama, K.; Nakanishi, H.; Uratsuji, Y.; Nomura, H.; Takeyama, Y.; Nishizuka, Y. Studies on the phosphorylation of myelin basic protein by protein kinase C and adenosine 3':5'-monophosphate-dependent protein kinase. *J. Biol. Chem.*, **1985**, *260*, 12492-12499.
- [55] Kuzuyama, T.; Takahashi, S.; Takagi, M.; Seto, H. Characterization of 1-deoxy-D-xylulose 5-phosphate reductoisomerase, an enzyme involved in isopentenyl diphosphate biosynthesis and identification of its catalytic amino acid residues. *J. Biol. Chem.*, **2000**, *275*, 19928-19932.
- [56] Zubrzycki, I.Z.; Blatch, G.L. DFT study of a substrate and inhibitors of 1-deoxy-D-xylulose-5-phosphate reductoisomerase - the potential novel target molecule for anti-malaria drug development. *J. Mol. Model.*, **2001**, *7*, 378-383.